

## Article

# Photocatalytic Properties of Amorphous N-Doped TiO<sub>2</sub> Photocatalyst under Visible Light Irradiation

Kyong-Hwan Chung <sup>1</sup>, Byung-Joo Kim <sup>2</sup> , Young-Kwon Park <sup>3</sup>, Sang-Chai Kim <sup>4</sup> and Sang-Chul Jung <sup>1,\*</sup> 

<sup>1</sup> Department of Environmental Engineering, Sunchon National University, 255 Jungang-ro, Suncheon 57922, Korea; likeu21@hanmail.net

<sup>2</sup> Department of Carbon & Nanomaterials Engineering, Jeonju University, 303 Cheonjam-ro, Jeonju 55069, Korea; kimbj2015@gmail.com

<sup>3</sup> School of Environmental Engineering, University of Seoul, 163 Seoulsiripdaero, Dongdaemun-gu, Seoul 02504, Korea; catalica@uos.ac.kr

<sup>4</sup> Department of Environmental Education, Mokpo National University, 1666 Cheonggye-myeon, Muan-gun 58554, Korea; gikim@mokpo.ac.kr

\* Correspondence: jsc@sunchon.ac.kr; Tel.: +82-61-750-3814

**Abstract:** Amorphous TiO<sub>2</sub> doped with N was characterized by its photocatalytic activity under visible light irradiation. The amorphous N-doped TiO<sub>2</sub> was prepared by the sol-gel method through heat treatment at a low temperature. The photocatalyst showing activity in visible light despite heat treatment at low temperature can be applied to plastics and has excellent utility. The N-doped TiO<sub>2</sub> appeared amorphous when heat-treated at 130 °C. It was converted into an anatase-type N-doped TiO<sub>2</sub> when this was calcined at 500 °C. The photocatalyst showed photocatalytic activities in the photocatalytic decomposition of formaldehyde and methylene blue under visible light irradiation. The photocatalyst exhibited a higher rate of hydrogen production than that of TiO<sub>2</sub> in photocatalytic decomposition of water under liquid-phase plasma irradiation. The bandgap of the amorphous N-doped TiO<sub>2</sub> measured by investigation of optical properties was 2.4 eV. The lower bandgap induced the photocatalytic activities under visible light irradiation.

**Keywords:** amorphous TiO<sub>2</sub>; nitrogen doping; photocatalytic activity; hydrogen production; visible light



**Citation:** Chung, K.-H.; Kim, B.-J.; Park, Y.-K.; Kim, S.-C.; Jung, S.-C. Photocatalytic Properties of Amorphous N-Doped TiO<sub>2</sub> Photocatalyst under Visible Light Irradiation. *Catalysts* **2021**, *11*, 1010. <https://doi.org/10.3390/catal11081010>

Academic Editors: Marta Gmurek and Anna Malankowska

Received: 22 June 2021

Accepted: 20 August 2021

Published: 21 August 2021

**Publisher's Note:** MDPI stays neutral with regard to jurisdictional claims in published maps and institutional affiliations.



**Copyright:** © 2021 by the authors. Licensee MDPI, Basel, Switzerland. This article is an open access article distributed under the terms and conditions of the Creative Commons Attribution (CC BY) license (<https://creativecommons.org/licenses/by/4.0/>).

## 1. Introduction

Pure TiO<sub>2</sub> has a high bandgap energy and can exhibit photocatalytic activity only in the UV region. The anatase TiO<sub>2</sub> requires a bandgap energy of about 3.2 eV. There have been many attempts to expand the photocatalytic activity of TiO<sub>2</sub> to the visible-light region [1–4]. Nitrogen doping among the various surface modification methods of TiO<sub>2</sub> has the advantages of ease of manufacture and eco-friendliness [5–7]. Nitrogen doping on TiO<sub>2</sub> can be prepared by a relatively simple method, and it has the advantage that N is doped on the most effective dopant due to its similar size to oxygen and metastable defect complex, as well as small ionization energy [8].

N-doped TiO<sub>2</sub> (N/TiO<sub>2</sub>) exhibits excellent photocatalytic activity as electrons in the valance band (VB) are excited to the conduction band (CB) even in the visible-light region [9,10]. Oxygen constituting the TiO<sub>2</sub> lattice is replaced by nitrogen, and it is known that it is located in a nitrogen oxide state between the TiO<sub>2</sub> lattice [11–14]. Anatase type TiO<sub>2</sub> has a bandgap energy of 3.2 eV, whereas N-doped or metal ion doped TiO<sub>2</sub> has a bandgap of 2.5 eV and 2.6 eV, respectively [15]. In other words, metal doping and nitrogen doping lower the bandgap so that electrons located in VB can transfer to CB even in the visible-light region [16,17]. The greatest advantage of impurity doping is the movement of hot electrons to CB even in visible light.

The N/TiO<sub>2</sub> photocatalyst obtained through a calcination at a high temperature of 400 °C or higher exhibits an anatase form. On the other hand, if the visible light-

response TiO<sub>2</sub> is manufactured by heat treatment at a low temperature of 150 °C or less, the manufacturing process can be simplified. In addition, when prepared with a photocatalytic coating solution according to the sol-gel method, a photocatalytic thin film is formed on the surface of the plastic and subjected to low temperature heat treatment to obtain photocatalytic activity.

For many years, research on modifying the structure of TiO<sub>2</sub> to expand the light absorption region of the TiO<sub>2</sub> photocatalyst to the visible ray region has been attracting attention. Many strategies have been attempted to extend the light absorption of TiO<sub>2</sub> to the visible light region, such as a method of coupling semiconductor materials having a narrow bandgap with TiO<sub>2</sub> and a method of doping various elements on TiO<sub>2</sub> [18–20]. These methods also increase the photocatalytic reaction efficiency by reducing the recombination of electrons and holes during the photoreaction of the TiO<sub>2</sub> photocatalyst [21,22]. Blocking the recombination of light-induced electron-hole pairs is part of an effort to maximize the utilization of solar energy and improve photocatalytic performance [23,24].

In general, the structure of TiO<sub>2</sub> crystallites is the most basic and essential property for predicting photocatalytic activity. Until now, most studies have focused on anatase-type TiO<sub>2</sub> crystallites. However, it has been found that amorphous TiO<sub>2</sub> contains more disorders and defects than those found in crystalline TiO<sub>2</sub> particles [25,26]. Therefore, amorphous TiO<sub>2</sub> is expected to be a promising candidate as a visible light-sensitive photocatalyst showing activity in visible light [27,28]. However, some studies have reported that amorphous TiO<sub>2</sub> exhibits photocatalytic activity only in weak ultraviolet light because most of the defects and materials on the surface can act as electron-hole traps [29,30]. Accordingly, a method of treating amorphous TiO<sub>2</sub> into a special microstructure by adding hydrogen to improve the photoactivity in visible light was also studied [31]. The study showed that modified TiO<sub>2</sub> has an irregular structure, which increases the edge of the VB and decreases the band gap, thereby improving the photocatalytic efficiency. It has also been reported that the photolysis of dyes can be greatly increased when metal ions and metal oxides are combined with amorphous TiO<sub>2</sub> [32,33].

In this study, TiO<sub>2</sub> doped with nitrogen was prepared as a visible light-sensitive photocatalyst. In the manufacturing process, amorphous N/TiO<sub>2</sub> was prepared by heat treatment at a low temperature of 130 °C. The physicochemical and optical properties of amorphous N/TiO<sub>2</sub> were investigated. The photocatalytic decomposition activity of HCHO and methylene blue (MB) was also evaluated under visible light irradiation. The hydrogen production property of N/TiO<sub>2</sub> was evaluated from water photocatalytic decomposition by liquid phase plasma (LPP) irradiation.

## 2. Results and Discussion

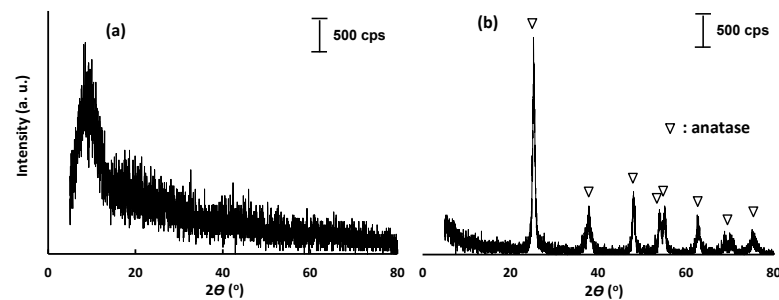
### 2.1. Physicochemical Properties of N/TiO<sub>2</sub>

Figure 1a shows the X-ray diffraction (XRD) pattern of N/TiO<sub>2</sub> heat-treated at 130 °C. The N/TiO<sub>2</sub> appeared as amorphous in the XRD pattern. When N/TiO<sub>2</sub> was calcined at 500 °C, the amorphous phase was changed to anatase phase as shown in Figure 1b. The presence of N in the TiO<sub>2</sub> structure will promote a peak broadening in XRD diffractograms compared to pure TiO<sub>2</sub>, which indicates a lower crystallite size of nanoparticles [34]. On the other hand, Barkul et al. [35] verified an increase in the crystallite size after N doping such that the increasing of the dopant load to at least 7% mol promoted higher crystallite sizes. This increase of the crystalline size was attributed to the higher intensity of the most significant peak (101). Therefore, no consensus can be found relative to the effect of the presence of nitrogen on the crystallite size. The crystallite size (*D*) is normally determined through the Scherrer equation:

$$D = \frac{k\lambda}{\beta \cos\theta} \quad (1)$$

where *k* is a shape factor that has a typical value between 0.89–0.94 [36],  $\lambda$  is the X-ray wavelength,  $\beta$  is the full width at half maximum peak (in radians), and  $\theta$  is the diffraction angle at which (101) and (110) intensity peaks appear [36]. This could be one explanation

for these differences in the crystallite sizes, since the  $k$  value can be attributed, and this equation only allows an estimated value for this parameter.



**Figure 1.** XRD patterns of N/TiO<sub>2</sub> calcined at 130 °C (a) and 500 °C (b).

Scanning electron microscope (SEM) images with energy dispersive X-ray spectroscopy (EDS) and transmission electron microscope (TEM) images of amorphous N/TiO<sub>2</sub> and anatase N/TiO<sub>2</sub> are shown in Figure 2. The amorphous N/TiO<sub>2</sub> particles showed an irregular spherical shape. It was difficult to accurately determine the size of the N/TiO<sub>2</sub> crystal because the crystals were agglomerated. The particle size obtained from the TEM image and the XRD peak is about 40 nm. The particles were clustered. The amount and size of the crystals of anatase N/TiO<sub>2</sub> were similar. The particle size of both N/TiO<sub>2</sub> was slightly larger than that of P25 TiO<sub>2</sub>.

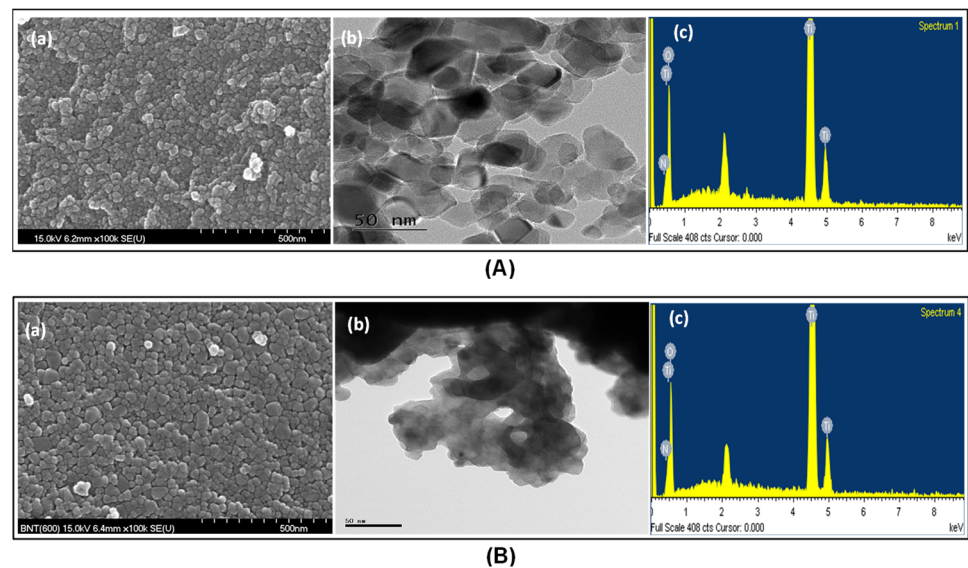


**Figure 2.** SEM-EDS and TEM images of (A) amorphous N/TiO<sub>2</sub> and (B) anatase N/TiO<sub>2</sub>: (a) SEM, (b) EDS, (c) TEM.

The thermal properties of the N/TiO<sub>2</sub> were investigated by thermo gravimetric analysis (TGA) and differential thermal analysis (DTA) at a temperature ranging from 25 °C to 1000 °C. The TGA/DTA pattern of the N/TiO<sub>2</sub> powder is shown in Figure 3. As the temperature increased, the most significant weight loss occurred before 500 °C, but the TGA curve was almost flat after 500 °C. The weight loss is due to the evaporation of water and residual organic solvents such as isopropanol below 160 °C. The weight loss is due to carbonization or combustion of organic components in the sol precursor at 200 °C to 500 °C. There was a slight weight loss after 500 °C.

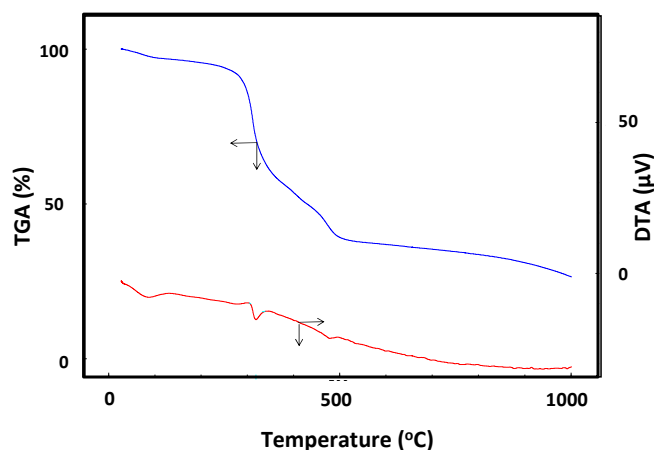


Figure 3. TGA/DTA results of amorphous N/TiO<sub>2</sub>.

Figure 4 shows N<sub>2</sub> isotherms of the P25 TiO<sub>2</sub>, amorphous N/TiO<sub>2</sub>, and anatase N/TiO<sub>2</sub>. The N<sub>2</sub> isotherm curve of P25 TiO<sub>2</sub> shows the curve for typical nonporous material. On the other hand, the N<sub>2</sub>-isotherm curves of both N/TiO<sub>2</sub> showed hysteresis type curves. The Brunauer-Emmett-Teller (BET) surface areas of both N/TiO<sub>2</sub> were smaller than that of P25. In previous results, it was shown that the particle size of N/TiO<sub>2</sub> was slightly increased as nitrogen was doped. It seems that it is because the surface of TiO<sub>2</sub> is doped by replacing O with N, so that the particle size is increased slightly and the adsorption amount of nitrogen is also decreased.

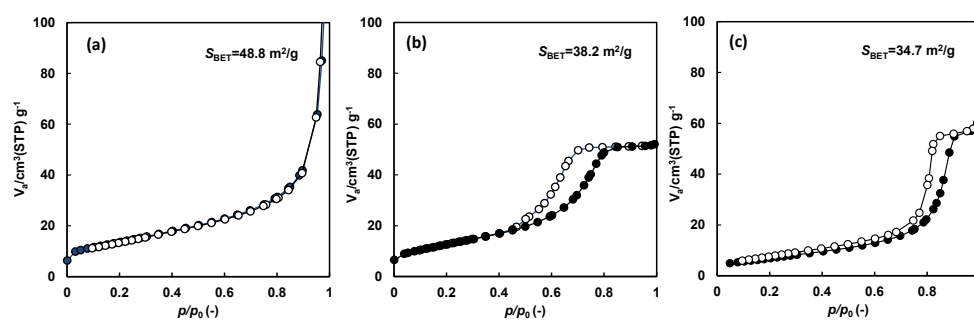


Figure 4. N<sub>2</sub> isotherms of (a) P25, (b) amorphous N/TiO<sub>2</sub>, and (c) anatase N/TiO<sub>2</sub>.

Figure 5 shows the FT-IR spectra of P25, amorphous TiO<sub>2</sub>, and anatase TiO<sub>2</sub>. The concentrated and broad band in the low wavenumber range between 500–800 cm<sup>-1</sup> common to all three samples is attributed to the strong stretching oscillations of Ti–O and Ti–O–Ti bonds [37]. Two peaks located at 3400 cm<sup>-1</sup> and 1620 cm<sup>-1</sup> were assigned to stretching vibrations of hydroxyl groups on the surface and OH bending of dissociated or molecularly adsorbed water molecules, respectively [38,39]. Compared with the band of P25, the intensity of both absorption bands was stronger in N/TiO<sub>2</sub>.

Figure 6 shows the results of X-ray photoelectron spectroscopy (XPS) to investigate the surface state of the amorphous N/TiO<sub>2</sub> and anatase N/TiO<sub>2</sub> particles. In XPS results of both N/TiO<sub>2</sub> particles, Ti2p, Ti2p<sub>3</sub>, Ti2p<sub>1</sub> peaks, O1s, and N1s peaks appeared. Ti2p<sub>1/2</sub> and Ti2p<sub>3</sub> peaks appeared at 463 eV and 457 eV binding energies, respectively. XPS results showed that N1s peaks were observed in the N/TiO<sub>2</sub> particle. The N1s peak was obtained at about 399 eV. The N1s peak at 399 eV was attributed to anionic N<sup>-</sup> in the form of N–Ti–O bond [40]. This suggests that nitrogen is doped on the surface of TiO<sub>2</sub>. N/TiO<sub>2</sub> doping with N atoms is an effective way to change the electronic structure of metal oxides. Both replacement and interstitial N-doping can significantly reduce the oxygen-void formation energy. In addition, doping with N atoms can lead to new single ionized oxygen vacancies. Comparing substitutional and interstitial N-doping can effectively narrow the bandgap.

When the N1s peak appeared near 398 nm in the XPS result, it was confirmed that N was introduced into TiO<sub>2</sub> to replace O [24]. This is most effective because the N2p electronic state is located just above the VB energy level of TiO<sub>2</sub>. This is described as substitutional type. The amorphous N/TiO<sub>2</sub> is also considered to be substitutional type, which is made by replacing O with N. N-doping can use visible light because N/TiO<sub>2</sub> absorbs 400 nm–650 nm visible light.

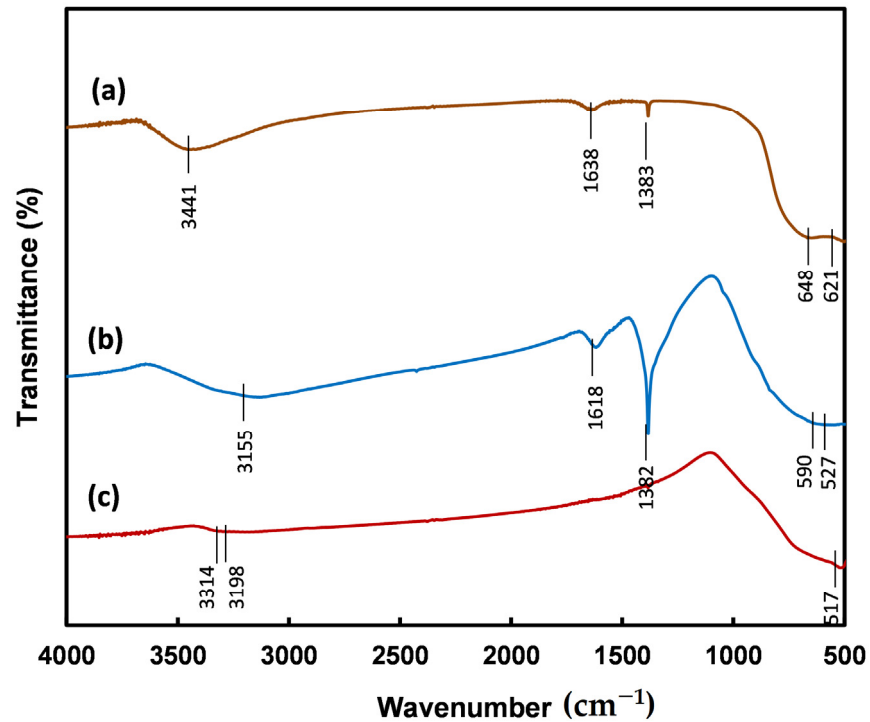


Figure 5. FT-IR spectra of (a) P25, (b) amorphous N/TiO<sub>2</sub>, and (c) anatase N/TiO<sub>2</sub>.

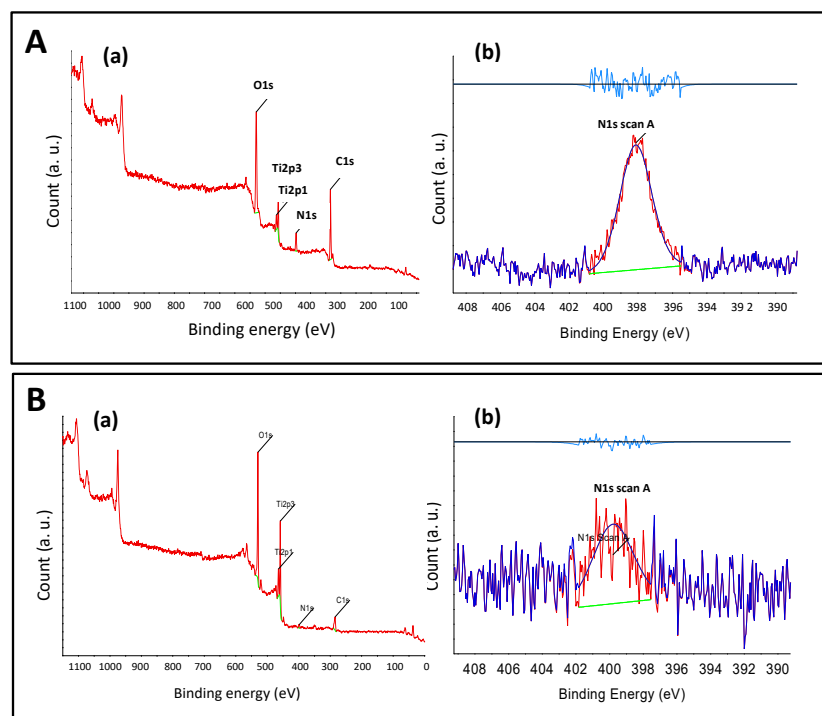


Figure 6. XPS spectra of (A) amorphous N/TiO<sub>2</sub> and (B) anatase N/TiO<sub>2</sub>; (a) full scan, (b) N1s scan.

Figure 7 shows the photoluminescence (PL) spectra of amorphous N/TiO<sub>2</sub> and anatase N/TiO<sub>2</sub>. The wavelength of the peak emission in this spectrum is converted into a bandgap by applying the equation  $E = hc/\lambda$ . The bandgap of both N/TiO<sub>2</sub> photocatalysts measured by this method were the same, about 2.4 eV. Anatase pure TiO<sub>2</sub> has a bandgap energy of 3.2 eV. As a result of N doping on TiO<sub>2</sub>, the bandgap was significantly reduced. The bandgap energy of titania doped with metal ions or nitrogen ions is significantly reduced. That is, metal doping or nitrogen doping narrows the band gap so that electrons located in VB can move to CB even by irradiation with visible light. Nitrogen doping is known to play a role in increasing VB energy. The migration of hot electrons to CB even in visible light is a result of impurity doping [41].

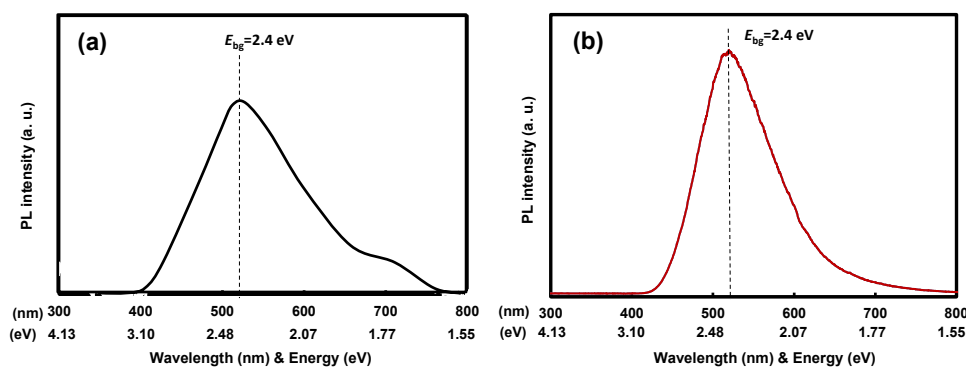


Figure 7. PL spectra of (a) amorphous N/TiO<sub>2</sub> and (b) anatase N/TiO<sub>2</sub>.

## 2.2. Photocatalytic Activity of the Amorphous N/TiO<sub>2</sub> under Visible Light Irradiation

Figure 8a shows the results of HCHO decomposition by the amorphous N/TiO<sub>2</sub> and visible LED lamp light. The decrease in the HCHO concentration due to the photocatalytic reaction is a value excluding the HCHO concentration that decreases due to adsorption on the inner surface of the test box without the lamp turned on. The concentration of HCHO concentration decreased as the photocatalytic decomposition reaction occurred by visible light by illuminating the LED lamp. The concentration of HCHO decreased in a curved shape over time. After 120 min, HCHO decreased by about 60% of the initial concentration. When the initial concentration was high, the decomposition rate increased slightly. Figure 7b shows the results of the decomposition reaction of MB in the N/TiO<sub>2</sub> photocatalyst. The tendency to decrease the concentration of MB was also high when the initial concentration was high. After 2 h of reaction time, the decomposition rate of MB was about 30%. Figure 8c represents the emitting spectrum of the LED lamp.

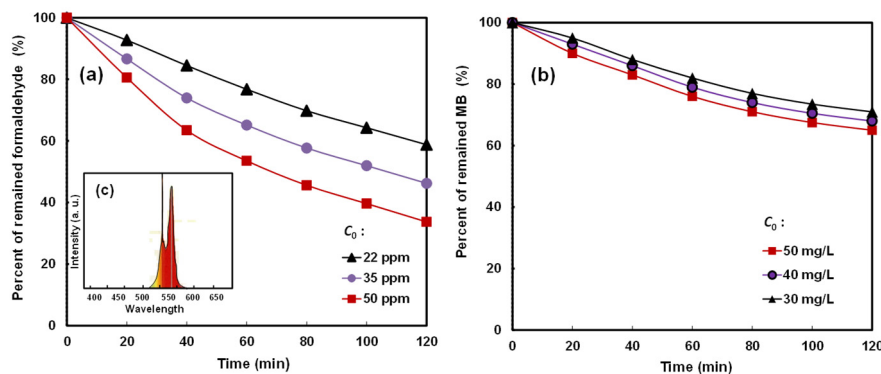


Figure 8. Visible light photocatalytic degradation of (a) HCHO and (b) MB with various  $C_0$  over N/TiO<sub>2</sub> photocatalyst. (c) Emitting spectrum of the LED visible light lamps.

Figure 9a illustrates the optical emission spectrum (OES) measured during plasma emission from water. The optical spectra obtained by LPP discharge in water showed

strong optical emission peaks such as  $H^{\beta}$  at 486 nm,  $H^{\alpha}$  at 656 nm, and  $O^1$  at 777 nm. The strongest emission peak appeared at 309 nm, which is indicated by the generation of a molecular band of OH radicals [42]. Another strong optical emission peak was also observed at 486 nm and 656 nm in the visible region. This means that LPP causes strong optical emission in the UV region and visible light region at the same time. Therefore, it suggests that the use of LPP can induce a photocatalytic reaction in the ultraviolet region and the visible-light region.

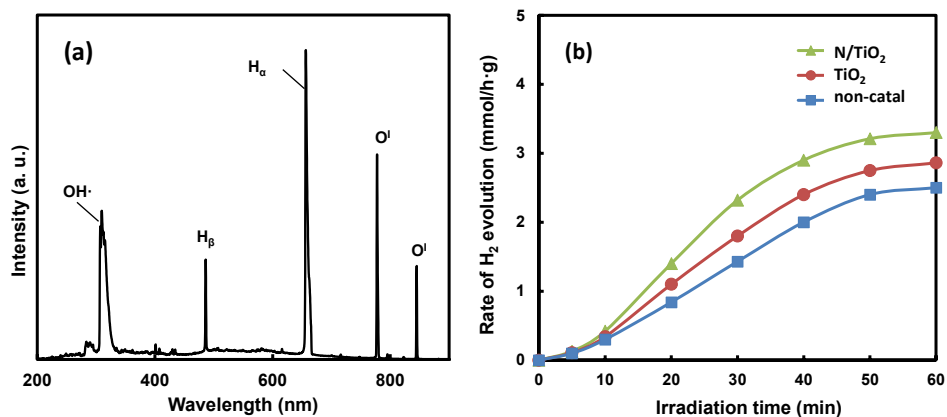


Figure 9. (a) OES of pure water and (b) rate of hydrogen evolution by LPP irradiation.

Figure 9b shows rates of H<sub>2</sub> evolution in the photocatalytic water decomposition under LPP irradiation. Hydrogen and a little oxygen were generated as gaseous products from the reaction. In the photochemical reaction of pure water using LPP, hydrogen gas was generated without injecting a photocatalyst. This shows the strong emissions by LPP irradiation, and it is presumed that ammonia and water are decomposed by the generated active species to generate hydrogen. As confirmed by the OES result, various active species were produced in large quantities by LPP irradiation. In particular, the OH radical acts as the main active species for hydrogen generation.

In this photochemical reaction, the hydrogen production rate was increased when P25 TiO<sub>2</sub> was injected. In the amorphous N/TiO<sub>2</sub>, the hydrogen production rate was further improved. The reason that the hydrogen production rate is high in the P25 is because the photocatalyst reacts to the light in the ultraviolet region emitted from the LPP. On the other hand, the hydrogen production rate was further improved in N/TiO<sub>2</sub>. This seems to be because N/TiO<sub>2</sub> reacts to strong visible light generated in the 486 nm and 656 nm regions as well as the ultraviolet light emitted from LPP. This is because, compared to TiO<sub>2</sub>, which has a bandgap of 3.2 eV, N/TiO<sub>2</sub> has a significantly narrower bandgap of 2.4 eV, which increases the photochemical reaction activity for visible light. It has been reported in the literature that amorphous TiO<sub>2</sub> prepared by the Stöber method exhibits higher photocatalytic activity than P25, which can clearly be attributed to the increased light absorption from 400 nm to 450 nm and the strong surface photovoltage spectroscopy response [43]. N/TiO<sub>2</sub> particles are amorphous and exhibit visible light sensitivity by N doping. Therefore, the photoreactive activity in visible light is higher than that of P25 crystal, which is sensitive only to UV light.

### 3. Materials and Methods

#### 3.1. Preparation of Amorphous N/TiO<sub>2</sub>

The N/TiO<sub>2</sub> was prepared by the following method: Ti{OCH(CH<sub>3</sub>)<sub>2</sub>}<sub>4</sub> (99%, Ducksan, Ansan, Korea) and 2-propanol (99%, Ducksan, Ansan, Korea) were added to distilled water to prepare a TiO<sub>2</sub> solution. The Ti{OCH(CH<sub>3</sub>)<sub>2</sub>}<sub>4</sub> content was adjusted to 10% based on the mass of TiO<sub>2</sub>. The solution was mixed at 20 °C for 4 h. This solution was poured into distilled water and hydrolyzed. (NH<sub>4</sub>)<sub>2</sub>CO<sub>3</sub> (30%, Samchun, Pyungtek, Korea) of 0.05 M was injected into the sol and stirred at the same temperature for 5 h to dope it with nitrogen.

This sol was heat-treated at 130 °C for 24 h in a muffle furnace (HYSC, MF-03, Seoul, Korea) to obtain N/TiO<sub>2</sub> powder. In the sol–gel reaction process, the synthesis was performed in a nitrogen atmosphere. The heat treatment of the sol precursor for the preparation of amorphous N/TiO<sub>2</sub> powder was carried out in an air atmosphere.

### 3.2. Characterization of the N/TiO<sub>2</sub> Photocatalyst

The crystallinity and structure of N/TiO<sub>2</sub> were measured by a high-resolution X-ray diffractometer (Rigaku, Maxii Ultimas III, The Woodlands, TX, USA). The morphology and microstructure of the N/TiO<sub>2</sub> were investigated by a scanning electron microscope (Hitachi, S-5000/EX-350, Tokyo, Japan). The chemical composition of the photocatalyst was analyzed by EDS using an energy dispersive X-ray spectrometer (NORANS Z-MAXII 350, Tokyo, Japan). Transmission electron microscopy (JEOL, JEM-2100F, Tokyo, Japan) was measured using a LaB<sub>6</sub> filament. The bonding state of the N/TiO<sub>2</sub> constituent elements was analyzed by X-ray photoelectron spectroscopy. The XPS was measured using an X-ray photoelectron spectrometer (VG, MultiLabs2000, London, UK). Photoluminescence was measured using a PL spectrophotometer (Spectrographs 5000i, Actons Research Co., Acton, MA, USA). A HeCd laser was applied for excitation at 266 nm. TGA and DTA measurements were carried out using a TGA/DSC (Shimadzu, TGA-50/DSC-60, Tokyo, Japan) instrument in nitrogen atmosphere with a heating rate of 10 °C/min. The N<sub>2</sub> isotherms of the photocatalysts were measured using a volume adsorption device (Mirae SI, Nanoporosity XQ, Gwangju, Korea) at liquid nitrogen temperature. The photocatalyst sample was pretreated at 100 °C for two hours and exposed to nitrogen gas. The surface area was calculated by applying the BET equation [44].

### 3.3. Evaluation of Visible Light Photocatalytic Properties of the Amorphous N/TiO<sub>2</sub>

Photocatalytic decomposition of the N/TiO<sub>2</sub> photocatalyst to HCHO and MB was performed under visible light irradiation. As a light source, an LED light source (12 W) combined with 585 nm and 613 nm LED lamps was used. The emission spectrum of the LED lamp appeared in the range of 580 nm to 640 nm. Photocatalytic decomposition of HCHO was carried out by installing an LED lamp inside a reaction box (V = 52.5 L). HCHO solution (40%, Deoksan, Ansan, Korea) was vaporized in a vaporizer. The vaporized HCHO was injected into the reaction box. A fan installed inside the reaction box was used to circulate the internal gas. After fixing the N/TiO<sub>2</sub> powder to the specimen, it was used for the reaction. The concentration of HCHO in the reaction was measured using gas chromatography (GC; Youngin, M6000D, Seoul, Korea). MB solution (100 mL) and N/TiO<sub>2</sub> (0.5 g) powder were injected into the reactor, and the LED lamp was irradiated while stirring. Changes in MB concentration were measured using a UV-visible spectrophotometer (Shimadzu UV-2450, Tokyo, Japan).

Hydrogen production was investigated from the photocatalytic reaction under LPP irradiation. The reactant was distilled water. A photocatalytic reaction was performed by directly irradiating the reactants with LPP in the photocatalytic reactor [45]. The temperature inside the LPP reactor was controlled at 20 °C by a water circulator. The generated gaseous product was measured for hydrogen generation with a mass flow meter (MFC Korea, TSM-D2200, Seoul, Korea) for measuring H<sub>2</sub> gas. The composition of the generated gas was analyzed by the GC equipped with a Molecular sieve 5A packing column. The LPP was radiated by a discharge system as a pulse discharge between the electrode needle and the needle [46]. The material of the electrodes was tungsten, and the distance between the electrodes was 0.2 mm. The pulse width range of the plasma generated by the discharge system was 3–5 μs and the frequency range of the plasma was 25–30 kHz. The optical emission spectroscopy the LPP was measured while emitting directly from the reaction using a fiber optical spectrometer (Avantes, AvaSpec-3500, Louisville, KY, USA).

#### 4. Conclusions

N/TiO<sub>2</sub> was prepared by a sol–gel method. The powder obtained by heat-treating it at 130 °C was amorphous N/TiO<sub>2</sub>. When this is calcined at 500 °C, it is converted to anatase N/TiO<sub>2</sub>. The band gap of amorphous N/TiO<sub>2</sub> and anatase N/TiO<sub>2</sub> was measured to be the same as 2.4 eV. This is significantly smaller than the band gap of pure TiO<sub>2</sub>. Amorphous N/TiO<sub>2</sub> showed photocatalytic activity in the decomposition reaction of HCHO and MB by visible light irradiation. N/TiO<sub>2</sub> showed a higher hydrogen production rate than pure TiO<sub>2</sub> in the photocatalytic decomposition of water by liquid plasma irradiation.

**Author Contributions:** K.-H.C. designed and performed the experiment. B.-J.K. and Y.-K.P. contributed to the analysis and the interpretation of data. S.-C.K. and S.-C.J. edited the original drafted paper. S.-C.J. supervised the experiments and paper. All authors have read and agreed to the published version of the manuscript.

**Funding:** This work was supported by a National Research Foundation of Korea (NRF) grant funded by the Korean Government (MSIT) (2021R1A2C1006315).

**Conflicts of Interest:** The authors declare no conflict of interest.

#### References

1. Asahi, R.; Morikawa, T.; Ohwaki, T.; Aoki, K.; Tago, Y. Visible-light photocatalysis in nitrogen-doped titanium oxide. *Science* **2001**, *293*, 269–271. [[CrossRef](#)]
2. Lee, S.S.; Kim, H.J.; Jung, K.T.; Kim, H.S.; Shul, Y.G. Photocatalytic activity of metal ion (Fe or W) doped titania. *Korean J. Chem. Eng.* **2001**, *18*, 914–918. [[CrossRef](#)]
3. Dong, C.; Song, H.; Zhou, Y.; Dong, C.; Shen, B.; Yang, H.; Matsuoka, M.; Xing, M.; Zhang, L. Sulfur nanoparticles in situ growth on TiO<sub>2</sub> mesoporous single crystals with enhanced solar light photocatalytic performance. *RSC Adv.* **2016**, *6*, 77863–77869. [[CrossRef](#)]
4. Gonell, F.; Puga, A.V.; Julian-Lopez, B.; Garcia, H. Copper-doped titania photocatalysts for simultaneous reduction of CO<sub>2</sub> and production of H<sub>2</sub> from aqueous sulfide. *Appl. Catal. B Environ.* **2018**, *180*, 263–270. [[CrossRef](#)]
5. Dagher, R.; Drogui, P.; Robert, D. Modified TiO<sub>2</sub> for environmental photocatalytic applications: A review. *Ind. Eng. Chem. Res.* **2013**, *52*, 3581–3599. [[CrossRef](#)]
6. Lin, Y.C.; Chien, T.E.; Lai, P.C.; Chiang, Y.H.; Li, K.L.; Lin, J.L. TiS<sub>2</sub> transformation into S-doped and N-doped TiO<sub>2</sub> with visible-light catalytic activity. *Appl. Surf. Sci.* **2015**, *359*, 1–6. [[CrossRef](#)]
7. Nakamura, R.; Tanaka, T.; Nakato, Y. Mechanism for visible light responses in anodic photocurrents at N-doped TiO<sub>2</sub> film electrode. *J. Phys. Chem. B* **2004**, *108*, 10617–10620. [[CrossRef](#)]
8. Park, C.H.; Zhang, S.B.; Wei, S.-H. Origin of *p*-type doping difficulty in ZnO: The impurity perspective. *Phys. Rev. B* **2002**, *66*, 073202. [[CrossRef](#)]
9. Oh, K.; Hwang, D.K. Brief review on the preparation of N-doped TiO<sub>2</sub> and its application to photocatalysis. *Korean Chem. Eng. Res.* **2019**, *57*, 331–337.
10. Nolan, N.T.; Synnott, D.W.; Seery, M.K.; Hinder, S.J.; Wassenhoven, A.V.; Pillai, S.C. Effect of N-doping on the photocatalytic activity of sol-gel TiO<sub>2</sub>. *J. Hazard. Mater.* **2012**, *211–212*, 88–94. [[CrossRef](#)]
11. He, T.; Zeng, X.; Rong, S. The controllable synthesis of substitutional and interstitial nitrogen-doped manganese dioxide: The effects of doping sites on enhancing the catalytic activity. *J. Mater. Chem. A* **2020**, *8*, 8383–8396. [[CrossRef](#)]
12. Ashkarran, A.A.; Hamidnezhad, H.; Haddadi, H.; Mahmoudi, M. Double-doped TiO<sub>2</sub> nanoparticles as an efficient visible-light-active photocatalyst and antibacterial agent under solar simulated light. *Appl. Surf. Sci.* **2014**, *301*, 338–345. [[CrossRef](#)]
13. Xiang, Y.; Wang, X.; Zhang, X.; Hou, H.; Dai, K.; Huang, Q.; Chen, H. Enhanced visible light photocatalytic activity of TiO<sub>2</sub> assisted by organic semiconductors: A structure optimization strategy of conjugated polymers. *J. Mater. Chem. A* **2018**, *6*, 153–159. [[CrossRef](#)]
14. Antony, R.P.; Mathews, T.; Ajikumar, P.K.; Krishna, D.N.; Dash, S.; Tyagi, A.K. Electrochemically synthesized visible light absorbing vertically aligned N-doped TiO<sub>2</sub> nanotube array films. *Mater. Res. Bull.* **2012**, *47*, 4491–4497. [[CrossRef](#)]
15. Asahi, R.; Morikawa, T.; Irie, H.; Ohwaki, T. Nitrogen doped titanium dioxide as visible-light-sensitive photocatalysts: Designs, developments, and prospects. *Chem. Rev.* **2014**, *144*, 9824–9852. [[CrossRef](#)] [[PubMed](#)]
16. Peng, F.; Cai, L.; Huang, L.; Yu, H.; Wang, H. Preparation of nitrogen-doped titanium dioxide with visible-light photocatalytic activity using a facile hydrothermal method. *J. Phys. Chem. Solids* **2008**, *69*, 1657–1664. [[CrossRef](#)]
17. Valentin, C.D.; Finazzi, E.; Pacchioni, G.; Selloni, A.; Livraghi, S.; Paganini, M.C.; Giamello, E. N-doped TiO<sub>2</sub>: Theory and experiment. *Chem. Phys.* **2007**, *339*, 44–56. [[CrossRef](#)]
18. Hexing, L.; Xinyu, Z.; Yuning, H.; Jian, Z. Supercritical preparation of a highly active S-doped TiO<sub>2</sub> photocatalyst for methylene blue mineralization. *Environ. Sci. Technol.* **2007**, *41*, 4410.

19. Zhang, J.; Wu, Y.; Xing, M.; Leghari, S.A.K.; Sajjad, S. Development of modified N doped TiO<sub>2</sub> photocatalyst with metals, non-metals and metal oxides. *Energy Environ. Sci.* **2010**, *3*, 715–726. [[CrossRef](#)]
20. Hu, X.; Qi, Z.; Wang, X.; Kawazoe, N.; Yang, Y. Nonmetal-metal-semiconductor-promoted P/Ag/Ag<sub>2</sub>O/Ag<sub>3</sub>PO<sub>4</sub>/TiO<sub>2</sub> photocatalyst with superior photocatalytic activity and stability. *J. Mater. Chem.* **2015**, *A3*, 17858–17865. [[CrossRef](#)]
21. Yu, J.C.; Jiang, Y.; Zhang, H. Effects of F-doping on the photocatalytic activity and microstructures of nanocrystalline TiO<sub>2</sub> powders. *Chem. Mater.* **2002**, *14*, 3808–3816. [[CrossRef](#)]
22. Hoang, S.; Berglund, S.P.; Hahn, N.T.; Bard, A.J.; Mullins, C.B. Enhancing visible light photo-oxidation of water with TiO<sub>2</sub> nanowire arrays via cotreatment with H<sub>2</sub> and NH<sub>3</sub>: Synergistic effects between Ti<sup>3+</sup> and N. *J. Am. Chem. Soc.* **2012**, *134*, 3659–3662. [[CrossRef](#)] [[PubMed](#)]
23. Liu, S.X.; Chen, X.Y. A visible light response TiO<sub>2</sub> photocatalyst realized by cationic S-doping and its application for phenol degradation. *J. Hazard. Mater.* **2008**, *152*, 48–55. [[CrossRef](#)] [[PubMed](#)]
24. Khaki, M.R.D.; Shafeeyan, M.S.; Raman, A.A.A.; Daud, W.M.A.W. Application of doped photocatalysts for organic pollutant degradation—A review. *J. Environ. Manag.* **2017**, *198*, 78–94. [[CrossRef](#)] [[PubMed](#)]
25. Khatim, O.; Amamra, M.; Chhor, K.; Bell, A.M.T.; Novikov, D.; Vrel, D.; Kanaev, A. Amorphous-anatase phase transition in single immobilized TiO<sub>2</sub> nanoparticles. *Chem. Phys. Lett.* **2013**, *55*, 53–56. [[CrossRef](#)]
26. Yi, C.; Liao, Q.; Deng, W.; Huang, Y.; Mao, J.; Zhang, B.; Wu, G. The preparation of amorphous TiO<sub>2</sub> doped with cationic S and its application to the degradation of DCFs under visible light irradiation. *Sci. Total Environ.* **2019**, *684*, 527–536. [[CrossRef](#)] [[PubMed](#)]
27. Henderson, M.A. A surface science perspective on TiO<sub>2</sub> photocatalysis. *Surf. Sci. Rep.* **2011**, *66*, 185–297. [[CrossRef](#)]
28. Huang, J.; Liu, Y.; Lu, L.; Li, L. The photocatalytic properties of amorphous TiO<sub>2</sub> composite films deposited by magnetron sputtering. *Res. Chem. Intermed.* **2012**, *38*, 487–498. [[CrossRef](#)]
29. Liang, J.; Wang, N.; Zhang, Q.; Liu, B.; Kong, X.; Wei, C. Exploring the mechanism of a pure and amorphous black-blue TiO<sub>2</sub>: H thin film as a photo anode in water splitting. *Nano Energy* **2017**, *42*, 151–156. [[CrossRef](#)]
30. Yue, L.; Takeshi, S.; Yoshiki, S.; Naoto, K. Hexagonal-close-packed, hierarchical amorphous TiO<sub>2</sub> nanocolumn arrays: Transferability, enhanced photocatalytic activity, and super amphiphilicity without UV irradiation. *J. Am. Chem. Soc.* **2010**, *40*, 14755–14762.
31. Jia, T.; Zhang, J.; Wu, J.; Wang, D.; Liu, Q.; Qi, Y.; Hu, B.; He, P.; Pan, W.; Qi, X. Synthesis amorphous TiO<sub>2</sub> with oxygen vacancy as carriers transport channels for enhancing photocatalytic activity. *Mater. Lett.* **2020**, *265*, 127465. [[CrossRef](#)]
32. Buddee, S.; Wongnawa, S.; Sirimahachai, U.; Puetpaibool, W. Recyclable UV and visible light photocatalytically active amorphous TiO<sub>2</sub> doped with M (III) ions (M = Cr and Fe). *Mater. Chem. Phys.* **2011**, *126*, 167–177. [[CrossRef](#)]
33. Tasbbihi, M.; Bendyna, J.K.; Notten, P.H.L.; Hintzen, H.T. A short review on photocatalytic degradation of formaldehyde. *J. Nanosci. Nanotechnol.* **2015**, *15*, 6386–6396. [[CrossRef](#)]
34. Lee, H.U.; Lee, S.C.; Choi, S.; Son, B.; Lee, S.M.; Kim, H.J.; Lee, J. Efficient visible-light induced photocatalyst on nanoporous nitrogen-doped titanium dioxide catalysts. *Chem. Eng. J.* **2013**, *228*, 756–764. [[CrossRef](#)]
35. Barkul, R.P.; Koli, V.B.; Shewale, V.B.; Patil, M.K.; Delekar, S.D. Visible active nanocrystalline N-doped anatase TiO<sub>2</sub> particles for photocatalytic mineralization studies. *Mater. Chem. Phys.* **2016**, *173*, 42–51. [[CrossRef](#)]
36. Sun, X.; Liu, H.; Dong, J.; Wei, J.; Zhang, Y. Preparation and characterization of Ce/N-Co-doped TiO<sub>2</sub> particles for production of H<sub>2</sub> by photocatalytic splitting water under visible light. *Catal. Lett.* **2010**, *135*, 219–225. [[CrossRef](#)]
37. Yu, J.G.; Yu, H.G.; Cheng, B.; Zhao, X.J.; Yu, J.C.; Ho, W.K. The effect of calcination temperature on the surface microstructure and photocatalytic activity of TiO<sub>2</sub> thin films prepared by liquid phase deposition. *J. Phys. Chem. B* **2003**, *107*, 13871–13879. [[CrossRef](#)]
38. Ren, L.; Huang, X.T.; Sun, F.L.; He, X. Preparation and characterization of doped TiO<sub>2</sub> nano-dandelion. *Mater. Lett.* **2007**, *61*, 427–431. [[CrossRef](#)]
39. Wang, J.W.; Zhu, W.; Zhang, Y.Q.; Liu, S.X. An efficient twostep technique for nitrogen-doped titanium dioxide synthesizing: Visible-light-induced photodecomposition of methylene blue. *J. Phys. Chem. C* **2007**, *111*, 1010–1014. [[CrossRef](#)]
40. Xu, J.H.; Li, J.X.; Dai, W.L.; Cao, Y.; Li, H.X.; Fan, K.N. Simple fabrication of twist-like helix N, S-codoped titania photocatalyst with visible-light response. *Appl. Catal. B Environ.* **2008**, *79*, 72–80. [[CrossRef](#)]
41. Tarasov, A.; Minnerkhanov, A.; Trusov, G.; Konstantinova, E.; Zyubin, A.; Zyubina, T.; Sadovnikov, A.; Dobrovosky, Y.; Doodilin, E. Shedding light on aging of N-doped titania photocatalysts. *J. Phys. Chem. C* **2015**, *119*, 18663–18670. [[CrossRef](#)]
42. Sun, S.H.; Jung, S.-C. Facile synthesis of bimetallic Ni-Cu nanoparticles using liquid phase plasma method. *Korean J. Chem. Eng.* **2016**, *33*, 1075–1079. [[CrossRef](#)]
43. Wang, Y.; Yang, H.; Zou, W. Preparation of amorphous sphere-like TiO<sub>2</sub> with excellent photocatalytic performance. *Mater. Lett.* **2019**, *254*, 54–57. [[CrossRef](#)]
44. Brunauer, S.; Emmett, P.H.; Teller, E. Adsorption of Gases in Multimolecular Layers. *J. Am. Chem. Soc.* **1938**, *60*, 309–319. [[CrossRef](#)]
45. Kim, S.-C.; Park, Y.-K.; Kim, B.H.; Kim, H.; Lee, W.-J.; Lee, H.; Jung, S.-C. Facile precipitation of tin oxide nanoparticles on graphene sheet by liquid phase plasma method for enhanced electrochemical properties. *Korean J. Chem. Eng.* **2018**, *35*, 750–756. [[CrossRef](#)]
46. Lee, W.-J.; Jeong, S.; Lee, H.; Kim, B.-J.; An, K.-H.; Park, Y.-K.; Jung, S.-C. Facile synthesis of iron-ruthenium bimetallic oxide nanoparticles on carbon nanotube composites by liquid phase plasma method for supercapacitor. *Korean J. Chem. Eng.* **2017**, *34*, 2993–2998. [[CrossRef](#)]